Shape transformations of a model of self-avoiding triangulated surfaces of sphere topology

Hiroshi Koibuchi

Department of Mechanical and Systems Engineering, Ibaraki National College of Technology, Nakane 866 Hitachinaka, Ibaraki 312-8508, Japan

koibuchi@mech.ibaraki-ct.ac.jp

We study a surface model with a self-avoiding (SA) interaction using the canonical Monte Carlo simulation technique on fixed-connectivity (FC) triangulated lattices of sphere topology. The model is defined by an area energy, a deficit angle energy, and the SA potential. A pressure term is also included in the Hamiltonian. The volume enclosed by the surface is well defined because of the self-avoidance. We focus on whether or not the interaction influences the phase structure of the FC model under two different conditions of pressure Δp; zero and small negative. The results are compared with the previous results of the self-intersecting model, which has a rich variety of phases; the smooth spherical phase, the tubular phase, the linear phase, and the collapsed phase. We find that the influence of the SA interaction on the multitude of phases is almost negligible except for the evidence that no crumpled surface appears under $\Delta p=0$ at least even in the limit of zero bending rigidity $\alpha\to 0$. The Hausdorff dimension is obtained in the limit of $\alpha\to 0$ and compared with previous results of SA models, which are different from the one in this paper.

Keywords: Triangulated surface model; Self-avoiding interaction; Monte Carlo; Shape transformations; Phase transitions

PACS Nos.: 11.25.-w, 64.60.-i, 68.60.-p, 87.10.-e, 87.15.ak

1. Introduction

Over the past few decades, a considerable number of studies have been conducted on the surface models. The model was constructed for strings and membranes [1,2,3,4,5,6,7], and it was defined on the basis of the differential geometric notion of curvatures [8,9,10,11]. The so-called crumpling transition is a shape transformation between the smooth phase at sufficiently large bending rigidity α and the collapsed phase at $\alpha\to 0$, and it has long been studied both theoretically [12,13,14,15] and numerically [16,17,18,19,20,21]. While the transition is considered as a continuous one [14,15], a possibility that it is of first-order is pointed out [13], and renormalization group studies [22] and recent numerical studies [23,24,25,26] predict that the transition is of first order. The transition was observed in the canonical surface model on relatively large sized surfaces [25].

In addition to the smooth and the collapsed phases, a variety of phases including the tubular phase are observed in surface models [27], which are defined by a one-dimensional bending energy on the cytoskeletal structure. A planar phase and an

oblong linear phase can be seen in a model [28], which is defined by a one-dimensional bending energy and the Nambu-Goto area energy on the fixed-connectivity (FC) surface. A surface model defined by a deficit angle energy also has a rich variety of phases including a tubular phase [29]. It must be noted that these phase transitions can be observed on relatively smaller surfaces in contrast to the above mentioned crumpling transition of the canonical surface model.

To construct a surface model, the self-avoiding (SA) property should be taken into account if we focus on membranes [31,32,33,34,35,36,37,38,39,40,41,42]. However, numerical studies of the SA surfaces are very time consuming because of the non-local property of the interactions. The simulations on such large surfaces like those in Refs. [25,26] are still not feasible on currently available computers. Nevertheless, the numerical studies on the above mentioned variety of phases in those specific models are considered to be feasible on the SA surfaces.

Therefore, it is very interesting to study whether or not the SA interaction influences the phase structure in those models without SA interactions (phantom surface models). It is possible that the multitude of phases is strongly influenced by the SA interactions. In fact, no completely-collapsed phase is observed in FC SA surfaces [33,34,35,36,37,38,42]. Moreover, the SA interaction is expected to play a non-trivial role in the membrane morphology even at the smooth phase. It was recently reported that SA property is essential for a variety of shapes of the so-called excess cone at high bending regime [43].

In this paper, we study the surface model in Ref. [29] with a SA interaction on FC triangulated surfaces by using the canonical Monte Carlo (MC) simulation technique. The smooth spherical phase, the tubular phase, the linear phase, and the collapsed phase are seen in the FC phantom surface model [29]. Our interests are focused on whether or not such a variety of phases, including the collapsed phase, are influenced by the SA interaction. Two different values of pressure Δp are assumed such that Δp is zero and small negative.

This paper is organized as follows: in Section 2, we make a brief outline of the current results of the numerical studies of phantom surface models and SA surface models on triangulated surfaces. In Section 3, we define the model with a SA interaction, which is slightly different from the currently well-known SA interactions for numerical studies. The Monte Carlo simulation technique is shown in Section 4, and the numerical results are presented in Section 5. We summarize the results in the final Section 6.

2. Triangulated surface models

2.1. *Phase structure of phantom surface models*

In this subsection, we give a brief outline of the phantom surface models on triangulated lattices in $\mathbf{R}^3$ and the current numerical results. We start with the continuous model, which is given by the continuous Hamiltonian $S = S_1 + \alpha S_2$, where $S_1 = \int \sqrt{g} d^2x g^{ab} \partial_a X^\mu \partial_b X^\mu$ and $S_2 = (1/2) \int \sqrt{g} d^2x g^{ab} \partial_a n^\mu \partial_b n^\mu$. S_1 is just iden-

tical with the action of Polyakov string [9,10], where X^μ denotes a mapping from a two-dimensional surface M to $\mathbf{R}^3$ and represents the surface position in $\mathbf{R}^3$, g^{ab} is the inverse of the metric tensor g_{ab} of M, and g is the determinant of g_{ab}. The variables (x_1, x_2) represent a local coordinate of M. The image $X(M)(\subset \mathbf{R}^3)$ is the surface, which is triangulated in numerical studies. The symbol n^μ in S_2 denotes a unit normal vector of $X(M)$, and S_2 is called the bending energy, and α is the bending rigidity.

If g_{ab} is fixed to the Euclidean metric δ_{ab} and $X(M)$ is triangulated by piecewise linear triangles, then we have $S = S_1 + \alpha S_2$, $S_1 = \sum_{ij} (X_i - X_j)^2$, $S_2 = \sum_{ij} (1 - \mathbf{n}_i \cdot \mathbf{n}_j)$, where $X_i (\in \mathbf{R}^3)$ in S_1 is the position of the vertex i, $\mathbf{n}_i$ in S_2 is a unit normal vector of the triangle i. The FC model is statistical mechanically defined by the partition function

$$Z_{\rm fix} = \int' \prod_{i=1}^{N} dX_i \exp\left[-S(X)\right], \qquad \text{(fixed)}, \tag{1}$$

where the prime in $\int' \prod_{i=1}^{N} dX_i$ denotes that the three-dimensional multiple integrations are performed by fixing the center of mass of the surface at the origin of $\mathbf{R}^3$ to remove the translational zero mode. We call the FC model defined by the energies S_1 and S_2 as the "canonical" surface model. It was reported that the canonical model on surfaces of sphere topology undergoes a first-order transition at finite α_c between the smooth phase at $\alpha \to \infty$ and the collapsed phase at $\alpha \to 0$ [25]. The role of the Gaussian bond potential S_1 is to make the mean bond length constant and, hence, S_1 can be replaced by a Lennard-Jones type potential [23] and also by a hard-wall potential [26]. In a surface model on triangulated lattices of the seminal paper Ref. [18] of Kantor and Nelson, S_1 is given by a hard-core and hard-wall potential. This type of potential can be used as a SA potential, which is described in the following sebsection.

A variation of the canonical model is obtained by replacing S_1 with the Nambu-Goto area energy $S_\Delta = \sum_\Delta A_\Delta$, where A_Δ is the area of the triangle Δ. S_Δ is also obtained from the above mentioned continuous Hamiltonian S_1 by fixing g_{ab} as the induced metric $g_{ab} = \partial_a X^\mu \partial_b X^\mu$ of the mapping X. We call a model as the Nambu-Goto surface model if the Hamiltonian includes S_Δ as the bond potential term. It is well-known that the Nambu-Goto model with the canonical bending energy $S_2 = \sum_{ij} (1 - \mathbf{n}_i \cdot \mathbf{n}_j)$ is ill-defined in the sense that no equilibrium configuration is obtained in the numerical simulations [44]. The ill-definedness comes from the fact that the area A_Δ is totally independent of the shape of Δ, and the oblong and very thin triangles, which are considered as singular triangles, dominate the surface configurations in the whole range of α. However, if the canonical bending energy S_2 is replaced by a deficit angle energy such as $S_2^{\rm int} = \sum_i (\delta_i - \phi_0)^2$ or $S_2^{\rm int} = \sum_i |\delta_i - \phi_0|$ [45,46,47], the model turns to be well defined except in the limit of $\alpha \to 0$ [29]. The symbol δ_i in $S_2^{\rm int}$ is the sum of internal angles of triangles meeting at the vertex i, and ϕ_0 is a constant and fixed to $\phi_0 = 2\pi$ if the surface is closed. The deficit angle

energy $S_2^{\rm int}=-\sum_i \log(\delta_i/2\pi)$ is possible on closed surfaces such as a sphere [29,48]. Those deficit angle energies are called as the intrinsic curvature energy. The reason of the variety of phases in the Nambu-Goto model with $S_2^{\rm int}$ [29] seems that both S_Δ and $S_2^{\rm int}$ are insensitive to the surface shape. In fact, S_Δ is independent of whether or not the surface is composed of almost-regular triangles or oblong triangles. $S_2^{\rm int}$ is also independent of whether the surface is planar or cylindrical. Nevertheless, both of the smooth phase and the collapsed phase are stable on the disk surface [49] and on the torus [50]. In this, paper we study the Nambu-Goto surface model with the intrinsic curvature $S_2^{\rm int}$.

We should comment on the reason why we use $S_2^{\rm int}=-\sum_i \log(\delta_i/2\pi)$ as the intrinsic curvature energy. The origin of $S_2^{\rm int}=-\sum_i \log(\delta_i/2\pi)$ is the measure factor q_i^σ in the integrations $\int'\prod_{i=1}^N dX_i q_i^\sigma$ in Z, where q_i is the coordination number of the vertex i and $\sigma(=3/2)$ is a constant [51]. By identifying q_i with δ_i and extending the constant σ to the variable coefficient α, we have the expression $-\alpha\sum_i \log(\delta_i)$. Including the normalization factor 2π, we have the curvature energy $S_2^{\rm int}=-\sum_i \log(\delta_i/2\pi)$.

We should also comment on the fact that the mean value of S_1 is constant such that $\langle S_1/N\rangle = 3/2$ even in the limit of $b\to 0$. The reason for $\langle S_1/N\rangle = 3/2$ is understood from the scale invariant property of the partition function [7]. In fact, by rescaling the integration variable in Z such that $X\to\lambda X$, we obtain $Z(\lambda)=\lambda^{3(N-1)}\int'\prod_{i=1}^N dX_i \exp\left[-S(\lambda X)\right]$, where $S(\lambda X)=\lambda^2 S_1+bS_2$. The scale invariance of Z indicates that $Z(\lambda)$ is independent of λ and, therefore, is represented by $\partial Z(\lambda)/\partial\lambda|_{\lambda=1}=0$. Thus, we have $\langle S_1/N\rangle = 3(N-1)/2N\simeq 3/2$.

A variety of phases can also be seen in a model, which is obtained by replacing S_1 and S_2 of the canonical model with S_Δ and the one-dimensional bending energy $S_2^{\rm 1\text{-}d}$, respectively [28]. In this case, $S_2^{\rm 1\text{-}d}$ is sensitive to the surface shape, while S_Δ is not as mentioned above.

A variation of the canonical model is obtained also by including fluidity, which represents a lateral diffusion of vertices [6,16,17,19,20,21]. This two-dimensional fluidity is defined on dynamically triangulated surfaces, where the triangulation $\mathcal{T}$ is considered as a dynamical variable of the model. The partition function of the model with fluidity is thus given by

$$Z_{\rm flu}=\sum_{\mathcal{T}}\int'\prod_{i=1}^N dX_i \exp\left[-S(X,\mathcal{T})\right], \qquad \text{(fluid)} \tag{2}$$

where $S(X,\mathcal{T})$ represents that S is dependent on the variables X and $\mathcal{T}$, and $\sum_{\mathcal{T}}$ represents the sum over all possible triangulations. In the fluid model corresponding to the canonical model, we cannot see the transition, which is seen in the canonical model on FC spherical surfaces. This is expected from the phase structure of compartmentalized fluid surfaces [52], where the lateral diffusion is allowed only inside the compartment, which is a sublattice structure on the surface. In this compartmentalized model, a first-order transition, which is considered to be identical to the

one in the canonical FC model, disappears if the compartment size L_C is increased. The homogeneous fluid surface is obtained from the compartmentalized fluid surface by maximizing L_C such that the surface is composed of a single compartment or the surface has no compartment. Thus, we understand that the transition, which is observed on the compartmentalized fluid surfaces at relatively small L_C, cannot be observed on the homogeneous fluid surfaces. The Nambu-Goto model with the intrinsic curvature energy is well-defined even on the fluid surfaces and has a variety of phases [30].

By combining two different sets of ball-spring systems, Boal and Seifert introduced a fluid surface model with cytoskeletal structures, which is a two-components network model for red cells [53]. If a curvature energy is introduced on the compartment in place of the canonical bending energy S_2 in the compartmentalized fluid surface model in Ref. [52], we have also fluid surface models with cytoskeletal structures [27]. A large variety of shape transformations are observed in such inhomogeneous fluid surface models, where the bond potential S_1 is the Gaussian bond potential, and the curvature energy S_2 is the one-dimensional bending energy $S_2^{1\text{–d}}$ defined only on the compartments, which are one-dimensional objects linked with junctions [27]. The phase structure depends on the elasticity at the junctions; a planar phase, and a tubular phase are observed in those models. The reason for such a variety of phases is closely connected to the cytoskeletal structure and the lateral diffusion of vertices. In fact, $S_2^{1\text{–d}}$ is considered to be insensitive to the surface shape, because $S_2^{1\text{–d}}$ is defined only on the compartments in contrast to the model in Ref. [28], where $S_2^{1\text{–d}}$ is defined all over the lattice. The surface shape is not always uniquely determined if the curvature is given only at small part of the surface, and moreover large surface fluctuations are expected in the compartmentalized model in Ref. [27] due to the lateral diffusion of vertices inside the compartments.

2.2. *Self-avoiding surface models*

The current studies that have been conducted on SA surfaces are considered to be still in the pioneer stage. In this subsection, we briefly comment on the existing SA surface models and the results of the numerical studies. The SA surface model is defined by a SA interaction, which is an extension of the Hamiltonian of the Edward model for polymers [3,4]. The phase structure of the SA models has been extensively studied [31,32,33,34,35,36,37,38,39,40,41,42], although the total number of studies are currently considered to be far smaller than those of the phantom surfaces.

We have two types of SA models for numerical studies: the ball-spring (BS) model and the impenetrable plaquette (IP) model. The BS model is defined on two-dimensional networks, which are composed of vertices and bonds connecting two nearest neighbor vertices by a hard-core and hard-wall potential [31,32]. The size of ball as the vertices and the length of spring as bonds are constrained such that no vertex can move from one side of a triangle to the other side. This SA potential of the BS model is defined between all pairs of vertices, however, the simulations are

slightly less time-consuming than those of the IP model. The SA interaction of the IP model is defined such that the triangles are constrained to avoid intersecting. Although the simulations of the IP model are relatively time consuming, the IP model seems advantageous to the BS model. In fact, two neighboring triangles i and j of the IP model can completely bend such that $1-\mathbf{n}_i \cdot \mathbf{n}_j = 2$, while in the BS model the bending angle θ_{ij} is constrained such that $\theta_{ij} < \theta_0$, where $\cos\theta_{ij} = \mathbf{n}_i \cdot \mathbf{n}_j$, and $\theta_0 (< \pi)$ is determined by the SA potential.

The crumpling transition is reported to disappear from the SA FC surfaces [33,34,35,36,37,38,42]; this is because no completely-collapsed phase appears in the SA FC surfaces. In fact, no crumpled phase is observed in both of the BS model [33,34,37] and the IP model [35,36,38,42]. To the contrary, the smooth phase is expected to remain unchanged from that of the phantom surfaces. However, numerical results are not always universal; in fact, the Hausdorff dimension of the IP model of [38] is $H \simeq 2.3$, while that of Ref. [42] is $H = 2.1(1)$, although both models are defined on the disk surface. As mentioned in the Introduction, it is possible that the SA interaction plays a non-trivial role in membrane shapes in the smooth phase [43]. Thus, we should study the SA model more extensively.

To summarize the comments including those in the previous subsection, we have several phantom surface models, which have a multitude of phases. The models are considered as non-trivial variations of the canonical surface model. The phase structures of almost all models have not yet been studied on the SA surfaces. The current understanding of the phase structure of SA surfaces are as follows: the crumpling transition disappears from the FC model, because the SA interaction prohibits the surfaces from collapsing in both of the BS model and the IP model. The smooth phase of the SA surfaces are considered to be almost identical to the smooth phase of the phantom surfaces, while the membrane shapes are expected to be influenced by the SA interaction under some specific conditions.

3. Model

In this section, we define a SA model, which corresponds to the phantom surface models in Refs. [29,30]. Triangulated lattices of sphere topology are assumed to define the model, and the lattices are constructed using the icosahedron. By splitting the edges and faces of the icosahedron, we have a lattice of size $N = 10\ell^2 + 2$, where ℓ is the devision number of an edge of the icosahedron. The coordination number q of vertices is $q = 6$ almost everywhere excluding 12 vertices of $q = 5$. The lattice is characterized by the three numbers N, $N_B (= 3N\text{–}6 = 30\ell^2)$, and $N_T (= 2N\text{–}4 = 20\ell^2)$, which are the total number of vertices, the total number of bonds, and the total number of triangles, respectively. The lattices used in Ref. [29] are random lattices, of which the coordination number is not always uniform and, they are slightly different from the lattices constructed as above. However, the phase structure of FC surface models is expected to be independent of the lattice structure [26].

The dynamical variable of the FC model is the position $X_i (\in \mathbf{R}^3)$ of the vertex

$i(= 1, \cdots, N)$. The partition functions of the model are given by Eq. (1). The Hamiltonian $S(X)$ is defined by a linear combination of the area energy S_1, a curvature energy S_2, the pressure term $-\Delta p\, V$, and a SA potential U, such that

$$
\begin{aligned}
&S(X) = S_1 + \alpha S_2 - \Delta p\, V + U, \\
&S_1 = \sum_{\Delta} A_{\Delta}, \quad S_2 = -\sum_{i} \log\left(\delta_i / 2\pi\right), \\
&U = \sum_{\Delta, \Delta'} U(\Delta, \Delta'), \quad U(\Delta, \Delta') = \begin{cases} \infty & \text{(triangles } \Delta, \Delta' \text{ intersect)}, \\ 0 & \text{(otherwise)}. \end{cases}
\end{aligned}
\tag{3}
$$

S_1 is the sum over the area A_{Δ} of triangle Δ. The symbol δ_i in S_2 is the sum of internal angle of triangles meeting at the vertex i. S_2 can be called a deficit angle energy, although S_2 is different from the sum of the deficit angle $\delta_i - 2\pi$ of the vertex i. If S_2 is defined without "log" and is given by $\sum_i (\delta - 2\pi)$, then S_2 depends only on the surface topology and is a constant on piece-wise linearly triangulated surfaces. However, S_2 in Eq. (3) is well-defined as a curvature energy because of the log function as mentioned in Section 2.1. The symbol $\alpha[kT]$ denotes the bending rigidity, where k is the Boltzmann constant and T is the temperature.

V is the volume enclosed by the surface, and Δp is the pressure which is defined by $\Delta p = p_{\rm in} - p_{\rm out}$, where $p_{\rm out}$ ($p_{\rm in}$) is the pressure outside (inside) the surface. If $p_{\rm out}$ is assumed to be $p_{\rm out} = 0$, then the positive (negative) Δp implies that $p_{\rm in}$ is positive (negative). We should note also that the volume V is well defined only if the surface is self-avoiding. V is bounded below such that $V \geq 0$ in the SA surfaces, while V can be negative in non SA surfaces.

1

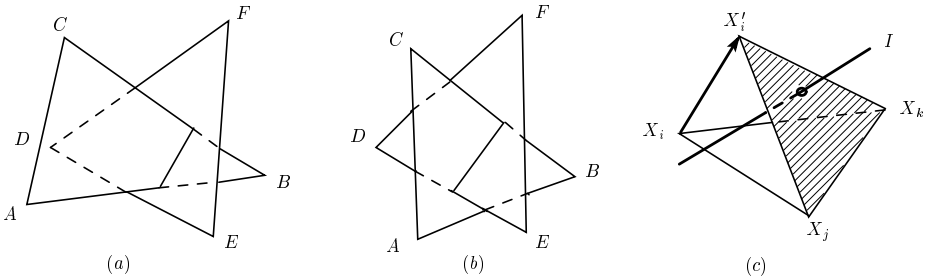

Fig. 1. (a),(b) Two intersecting triangles, and (c) an intersection of the bond I and the triangles with the vertices X_i', X_j and X_k, where X_i' is a new position of the vertex i. In (a), the bonds AB and BC of the triangle ABC intersect with the triangle DEF, while no bond of the triangle DEF intersects with the triangle ABC. In (b), the bond BC of the triangle ABC intersects with the triangle DEF, and the bond DE of the triangle DEF intersects with the triangle ABC.

$\sum_{\Delta, \Delta'}$ in the SA potential U denotes the sum over all pairs of non nearest neighbor triangles Δ and Δ'. The potential $U(\Delta, \Delta')$ is defined such that any pairs of non nearest neighbor triangles Δ and Δ' should not be intersecting. Figure 1(a)

shows two pairs of intersecting triangles, in which the triangle ABC penetrates the triangle DEF or in other words the bonds AB and BC intersect with the triangle DEF. On the contrary in Fig. 1(b), the triangle ABC and the triangle DEF intersects with each other, or in other words a bond of one triangle intersects with the other triangle and vise versa. We describe the numerical implementation of the SA interaction U in detail in the following section.

The SA potential U in Eq. (3) is not identical to the one assumed in the SA model in Ref. [42] and, hence, the surface is completely self-avoiding under the potential U. In fact, the triangles are allowed to intersect with finite energy in Ref. [42], while those in the model of this paper are prohibited to intersect with each other because of the infinite energy assumed in U.

Finally in this section, we comment on how to compute the volume V enclosed by the surface. The initial value of V in the simulations is assumed such that $V=4\pi r^3/3$, where r is the radius of the initial configuration of sphere lattice. This initial value $V=4\pi r^3/3$ is slightly larger than the real volume, because the surface is linearly triangulated. However, it is almost evident that the deviation can be negligible in the limit of $N\to\infty$. The volume V changes during the simulations according to the rule $V\to V+\Delta V$ every update of vertex, where ΔV is the volume of small tetrahedra, such as the one shown in Fig. 1(c). ΔV is positive or negative, which is determined according to whether the new position X_i' is outside or inside the surface, in which the orientation is uniquely fixed by a normal vector of each triangle. We should note that ΔV is well defined only when the surface is self-avoiding. It is apparent that ΔV is not well defined when some part of volume element of ΔV is shared by some other $\Delta V'$, i.e., the surface is allowed to self intersect.

The enclosed volume V can also be computed by using the divergence theorem applying the position vector $\mathbf{r}_i$ of the center of mass of the triangle i. Not only ΔV but also V is exactly identical to the one obtained by the above mentioned technique. A very small deviation can be seen in the total volume V, however, it is less than 1% even in the cup like phase on the $N=1442$ surface during the simulations. This small deviation of V is the one between $V=4\pi r^3/3$ and V of the initial triangulated sphere.

4. Monte Carlo technique

The canonical Metropolis Monte Carlo (MC) technique is employed for simulating the integrations of the variables X in $Z_{\rm fix}$ of Eq. (1). The three-dimensional random move $X\to X'=X+\delta X$ is accepted with the probability $\mathrm{Min}[1,\exp(-\delta S)]$, where δS is given by $\delta S=S(\mathrm{new})-S(\mathrm{old})$ under the constraint of the potential U. The symbol δX is randomly chosen in a small sphere, whose radius is fixed in the simulations such that the acceptance rate r_X of X' should be approximately $r_X=50\%$.

The constraint of $U(\Delta,\Delta')$ in Eq. (3) is composed of two different constraints on a new vertex position as follows: let X_i and X_i' denote the current position and

the new position of the vertex i as shown in Fig. 1(c). The shaded triangle in Fig. 1(c) forms a new surface. One of the constraint imposed on X_i' is that the new triangle $i'jk$ has no intersection with the disjoint bonds, where "disjoint bonds" are the edges of triangles disconnected with the triangle ijk. The other constraint is that every new bond, such as the bond $i'j$ in Fig. 1(c), has no intersection with the disjoint triangles, where "disjoint triangles" are those disconnected with the bond ij. These two constraints imposed on X_i' make the surface self-avoiding in the sense that any two disjoint triangles have no intersection with each other.

The first constraint prohibits the new triangle $i'jk$ shown in Fig. 1(c) from being penetrated by disjoint triangles. The second constraint imposed on X_i' prohibits the new triangle $i'jk$ from penetrating some other triangles. The intersection of the triangles shown in Fig. 1(b) is prohibited by both of the constraints, while the intersection in Fig. 1(a) is prohibited only by one constraint and is not prohibited by the other constraint. This is the reason why two constraints are necessary to make the surface self-avoiding by checking an intersection of a bond and a triangle.

We assume a sphere of radius R_0 at the center of mass of the triangle $i'jk$ shown in Fig. 1(c), and check whether or not the triangle intersects with disjoint bonds inside the sphere. The check of intersection in the second constraint is also performed assuming the sphere of size R_0 at the center of the bond $i'j$. The radius R_0 is assumed to be $R_0 = 6\langle L\rangle$, where $\langle L\rangle$ is the mean bond length. As a consequence, the computational time is reduced by $20\% \sim 60\%$ or more, which depends on α.

The bond length L and the triangle area A_Δ are bounded below such that $L > 1\times10^{-7}$ and $A_\Delta > 0.5\times10^{-7}$ in the simulations. The final results of the simulations are considered to be independent of these lower bounds, because these bounds are sufficiently small and almost all bond lengths and triangle areas are larger than these values.

The total number of MC sweeps (MCS) after the thermalization MCS is about $1\times10^7 \sim 2\times10^7$ on the $N = 1442$ surface, and relatively small number of MCS is assumed on the smaller surfaces. The total number of the thermalization MCS is about 0.5×10^6. The thermalization MCS in the collapsed tubular phase is very large; it is sometimes 1×10^7 or more at the phase boundary close to the cup like phase on the $N = 1442$ surface. Intersection of bonds with triangles is checked every 5×10^5 MCS throughout the simulation; the check is performed between every disjoint pair of bond and triangle. No intersection is observed at every assumed value of α including $\alpha = 0$ and Δp.

5. Results

The snapshots of FC surfaces at $\Delta p = 0$ are shown in Figs. 2(a)–2(f). The surface size is $N = 1442$. The assumed bending rigidities are (a) $\alpha = 0$, (b) $\alpha = 100$, (c) $\alpha = 500$, (d) $\alpha = 1000$, (e) $\alpha = 1\times10^4$, and (f) $\alpha = 2\times10^4$. The scales of the figures are all different from each other. The surfaces shown in the figure are considered to be in (a),(b),(c) the wrinkled phase, (d),(e) the tubular phase, and (f) the smooth

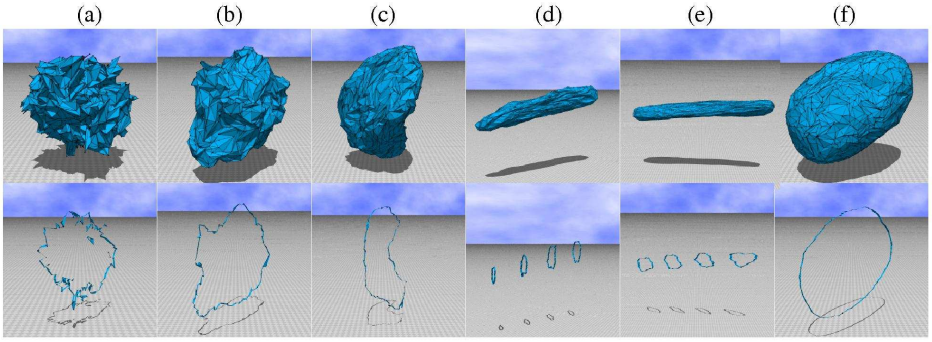

Fig. 2. The snapshots of FC surfaces and the surface sections of size $N = 1442$ obtained under $\Delta p = 0$ at (a) $\alpha = 0$ (wrinkled), (b) $\alpha = 100$ (wrinkled), (c) $\alpha = 500$ (wrinkled), (d) $\alpha = 1000$ (tubular), (e) $\alpha = 1 \times 10^4$ (tubular), and (f) $\alpha = 2 \times 10^4$ (smooth spherical).

spherical phase. The surface in Fig. 2(a) can be called a collapsed surface because the surface is highly fluctuating, however, it encloses empty space inside the surface and, therefore, the surface is not always crumpled in the limit of $\alpha \to 0$. The spherical surfaces in Figs. 2(b) and 2(c) look slightly smooth, however, they are apparently different from the surface at sufficiently large α shown in Fig. 2(f). The surfaces in Figs. 2(d) and 2(e) can be called a tubular surface. The surface in Fig. 2(f) is very smooth and can be called the smooth spherical surface. All of the phases, excluding the wrinkled phase, correspond to those of the same model without the SA interaction in Ref. [29]. The collapsed phase can be seen in the model in Ref. [29], while it is not in the SA model at least under $\Delta p = 0$.

Snapshots of the FC surfaces and the surface sections are shown in Figs. 3(a)–3(f), where a negative pressure $\Delta p = -0.5$ is assumed. The snapshots are slightly different from those at $\Delta p = 0$ shown in Figs. 2(a)–2(f). The snapshots in Figs. 3(a) and 3(b) indicate that the surfaces in the collapsed phase are almost crumpled. We see that the tubular surface in Fig. 3(c) is also collapsed. The cup like surfaces in Figs. 3(d) and 3(e) are new and typical of the condition $\Delta p = -0.5$, therefore, we call the new phase as the cup like phase. The smooth phase in Fig. 3(f) corresponds to the smooth phase in Fig. 2(f) at $\Delta p = 0$. The phase structure at $\alpha \to \infty$ is understood to be independent of Δp.

We also see that almost all parts of the surfaces in Figs. 2(d) and 2(e) consist of oblong triangles and are locally smooth along one specific direction and wrinkled along the direction vertical to the smooth direction. This is also expected in the linear phase shown in Fig. 3(c) at $\Delta p = -0.5$. To the contrary, the surface in the wrinkled phase shown in Fig. 2(a) consist of almost regular triangles and locally wrinkles along any directions. In the case of smooth phase in Fig. 2(f), the surface is smooth along any directions. Thus, the surface is symmetric under the three-dimensional rotations both in the limit of $\alpha \to \infty$ and $\alpha \to 0$, while the rotational symmetry is spontaneously broken at intermediate region of α. This observation

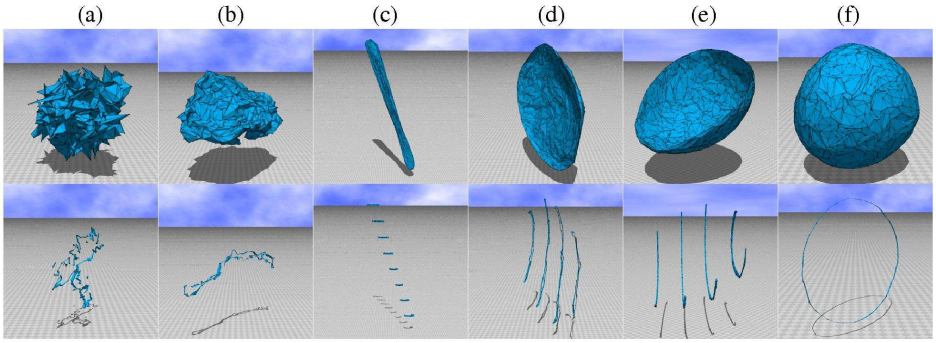

Fig. 3. The snapshots of FC surfaces and the surface sections of size $N = 1442$ obtained under $\Delta p = -0.5$ at (a) $\alpha = 0$ (collapsed), (b) $\alpha = 100$ (collapsed), (c) $\alpha = 1.5 \times 10^4$ (collapsed tubular), (d) $\alpha = 2 \times 10^4$ (cup like), (e) $\alpha = 3 \times 10^5$ (cup like), and (f) $\alpha = 4 \times 10^5$ (smooth spherical).

is independent of the two values of Δp. This symmetry breakdown or restoration is considered to be closely connected to the structural change of the constituent triangles; the symmetric surfaces are composed of almost regular triangles, while the non-symmetric surfaces are composed of oblong triangles.

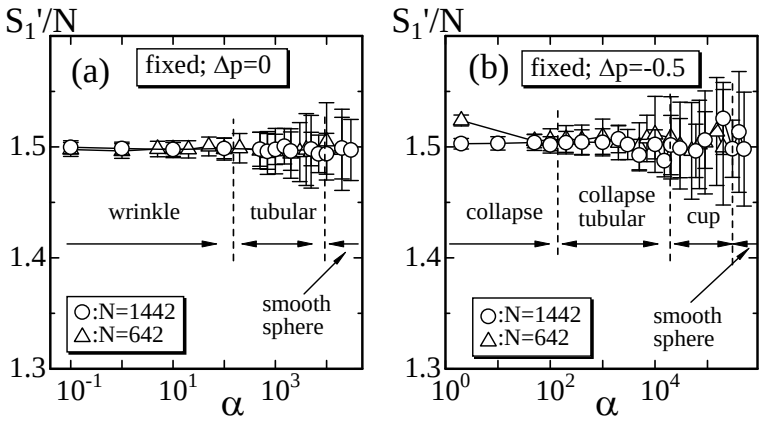

Fig. 4. $[S_1 - (3/2)\Delta p\, V]/N$ vs. α under (a) $\Delta p = 0$ and (b) $\Delta p = -0.5$. The error bars on the symbols denote the standard errors. The solid lines connecting the symbols are drawn as a guide to the eyes.

In the following presentations, we show how the shape transformation transitions and/or the SA interaction are reflected in the physical quantities including the Hausdorff dimension H in the limit of $\alpha \to 0$.

First of all, we show $[S_1 - (3/2)\Delta p\, V]/N$, denoted by S_1'/N, in Figs. 4(a) and 4(b). Because of the scale invariant property of the partition function $Z_{\rm fix}$ of Eq. (1), S_1'/N is expected to be $S_1'/N = 3/2$ at sufficiently large N. We see that all of the results are consistent with the prediction. This implies that the volume V is well-defined and that the SA interaction is correctly implemented in the simulations. We note that it is straightforward to prove that $S_1'/N = 3/2$ [7]. As described in Section 2.1, the scale invariance of Z is represented by $\partial Z(\lambda X)/\partial\lambda|_{\lambda=1} = 0$. Because of the scale transformation $X \to \lambda X$, S_1 and V change to $\lambda^2 S_1$ and $\lambda^3 V$ while S_2 and U remain unchanged. Since the integration $\int \prod_i dX_i$ also changes to $\lambda^{3(N-1)} \int \prod_i dX_i$, then we have the relation $S_1'/N = 3/2$ in the limit of $N \to \infty$.

S_1' is identical with S_1, which is the total area of surface, in the case $\Delta p = 0$, and therefore, the scale invariance implies that the surface area remains unchanged in the whole range of α. To the contrary, the surface area S_1 discontinuously changes at the transition points in the case $\Delta p = -0.5$ at least, because V discontinuously changes at the transitions as we will see below, while S_1' remains unchanged. This implies that the internal property of surface is significantly influenced by the external condition Δp.

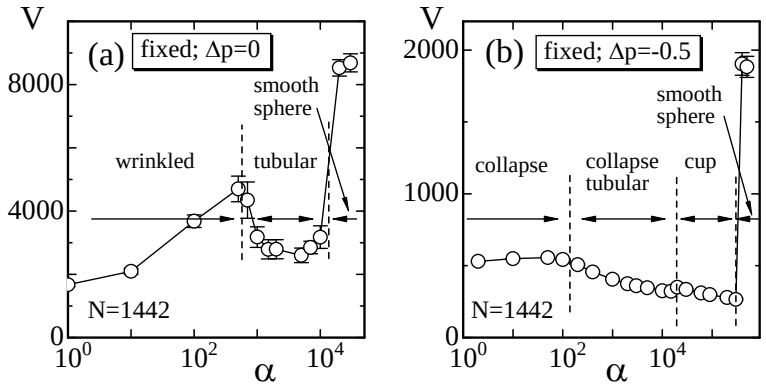

Fig. 5. The volume V vs. α under (a) $\Delta p = 0$ and (b) $\Delta p = -0.5$. The vertical dashed lines denote the phase boundaries of the $N = 1442$ surface. The solid lines connecting the symbols are drawn as a guide to the eyes.

The volume V enclosed by the surface should be bounded below such that $V \geq 0$, which is satisfied only if the surface is self-avoiding. The model in this paper is strictly self-avoiding, and hence V is expected to be well defined even when Δp is large negative. Figures 5(a) and 5(b) show the dependence of V on α under $\Delta p = 0$ and $\Delta p = -0.5$, respectively. The vertical dashed lines in the figures represent the phase boundaries between two different phases just like in Fig. 4. The name of the

phases corresponds to the surface shape, which can be visualized as snapshots just like those in Figs. 2 and 3.

The detailed informations such as the order of the transitions are not obtained. It is possible to perform the finite-size scaling analyses to see the order of the transitions by performing the simulations at the transition region more extensively, however, we confine ourselves of the phase structure in the wide range of α and, as a consequence, the order of the transitions is not fully examined. Thus, it remains unclear whether or not the smooth spherical phase and the tubular phase (or the cup like phase) are separated by a first-order transition, although the volume V discontinuously changes at the phase boundary. We see that the volume V in the collapsed phase is larger than that in the cup like phase under $\Delta p = -0.5$ at least, while V at $\alpha \to 0$ is smaller than that in the tubular phase under $\Delta p = 0$.

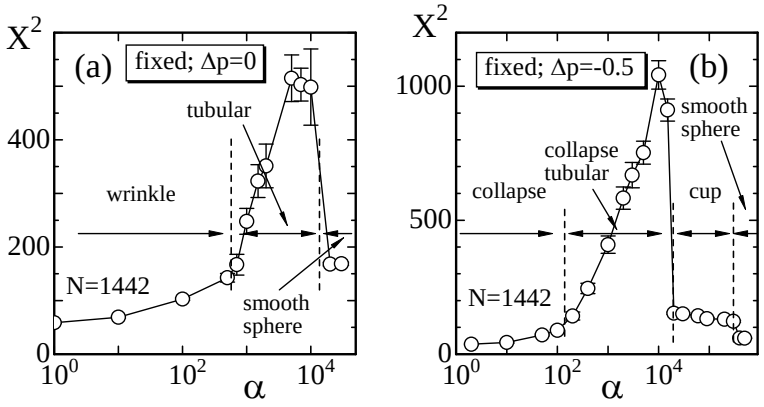

Fig. 6. The mean square size X^2 vs. α. The vertical dashed lines denote the phase boundaries of the $N = 1442$ surface.

The mean square size X^2 is defined by

$$X^2 = \frac{1}{N} \sum_i \left(X_i - \bar{X} \right)^2, \quad \bar{X} = \frac{1}{N} \sum_i X_i, \tag{4}$$

where $\bar{X}$ is the center of mass of the surface. The value of X^2 changes depending on the distribution of the vertices in $\mathbf{R}^3$, and hence X^2 as well as V can reflect shape transformations. However, the quantity X^2 does not always show the same behavior against α as that of V. Figures 6(a) and 6(b) show X^2 vs. α under $\Delta p = 0$ and $\Delta p = -0.5$. We see in Fig. 6(a) that X^2 discontinuously changes at the phase boundary between the smooth spherical phase and the tubular phase. It is also easy to see from Fig. 6(b) that X^2 discontinuously changes at the phase boundaries between the smooth spherical phase, the cup like phase, and the collapsed tubular phase.

Figures 7(a) and 7(b) show X^2 obtained under $\Delta p = 0$ and $\Delta p = -0.5$ at small

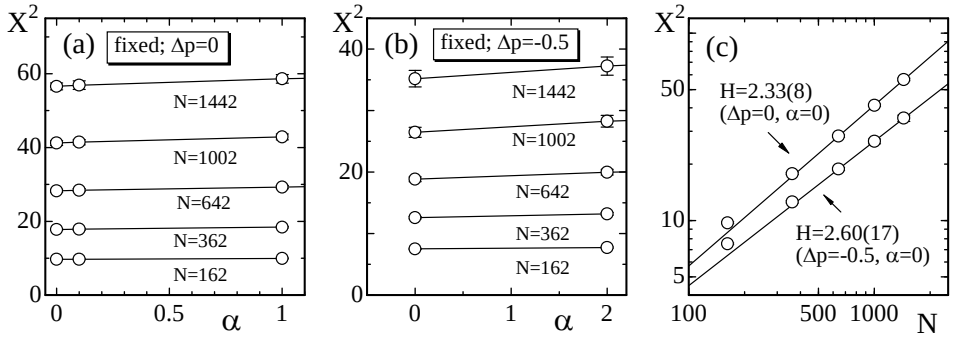

Fig. 7. The mean square size X^2 vs. α at small α region under (a) $\Delta p=0$ and (b) $\Delta p=-0.5$, and (c) X^2 vs. N in a log-log scale obtained at $\alpha=0$ under $\Delta p=0$ and $\Delta p=-0.5$. The straight lines in (c) are drawn by fitting the largest three data points to Eq.(5).

	$\alpha=0$	$\alpha=0.1$	$\alpha=1$	$\alpha=2$
$\Delta p=0$	$H=2.33\pm0.08$	$H=2.34\pm0.08$	$H=2.33\pm0.08$	-
$\Delta p=-0.5$	$H=2.60\pm0.17$	-	-	$H=2.59\pm0.17$

α region. The Hausdorff dimension H of the surface is defined by

$$X^2 \sim N^{2/H} \quad (N \to \infty). \tag{5}$$

By fitting the data X^2 obtained at $\alpha=0$ to Eq. (5), we draw straight lines in Fig. 7(c), and the values of H are shown in Table 1 including H at $\alpha=0.1$ and $\alpha=1$ under $\Delta p=0$, and at $\alpha=2$ under $\Delta p=-0.5$. The fitting is performed using the largest three data points under each condition of Δp. We have $H\simeq 2.6$ at $\Delta p=-0.5$ and $H\simeq 2.33$ at $\Delta p=0$ in the limit of $\alpha\to 0$. The value of $H\simeq 2.33$ is compatible with the one $H\simeq 2.3$ in Ref. [38], while $H\simeq 2.6$ at $\Delta p=-0.5$ is slightly larger than the Flory estimate 2.5 and compatible with the fact that the surface is almost crumpled as we see in the snapshot in Fig. 3(a). We should note that the value $H\simeq 2.3$ seems independent of the details of the model, the SA interaction, and the surface topology. However, the result $H\simeq 2.33$ is larger than the one $H=2.1(1)$ of Ref. [42], thus it is also possible that H depends on the model on the SA surfaces.

We comment on the size effect of the results in Table 1. As mentioned above, the data obtained on the small sized surfaces, such as $N=162$ and $N=362$, were excluded from the fitting. By including the small two data in the fitting, we have $H=2.50(5)$ for $\Delta p=0$, $\alpha=0$ and $H=2.93(7)$ for $\Delta p=-0.5$, $\alpha=0$. Both of H are slightly larger than $H=2.33(8)$ and $H=2.60(17)$ shown in Table 1. Thus, the size effect is not negligible at least on the surfaces $N\leq 362$.

The surface size can also be reflected in the maximum linear extension L_E, which is defined by the maximum distance between two vertices on the surface:

$$L_E = \mathrm{Max}\{|X_i - X_j| \mid (i,j=1,\cdots,N)\}, \tag{6}$$

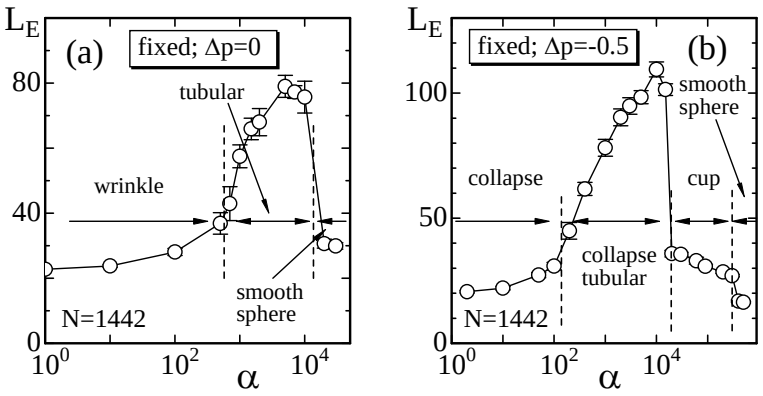

Fig. 8. The maximum linear extension L_E vs. α. The dashed lines denote the phase boundaries of the $N=1442$ surface.

where X_i and X_j are not always connected by a bond. The phase transition of shape transformation is also reflected in the structure of triangles; we see in the snapshots in Figs. 2 and 3 that the surface consists of almost regular triangles in the smooth spherical phase while it includes oblong triangles in the tubular phase, where L_E expected to be very large. We expect that this structural change is reflected in L_E. Figures 8(a) and 8(b) show L_E vs. α under $\Delta p=0$ and $\Delta p=-0.5$. The discontinuous change of L_E at the phase boundaries shown in the figure implies that the phase transitions are accompanied by the structural change of surfaces. This structural change is typical of the Nambu-Goto surface model [28,29,30].

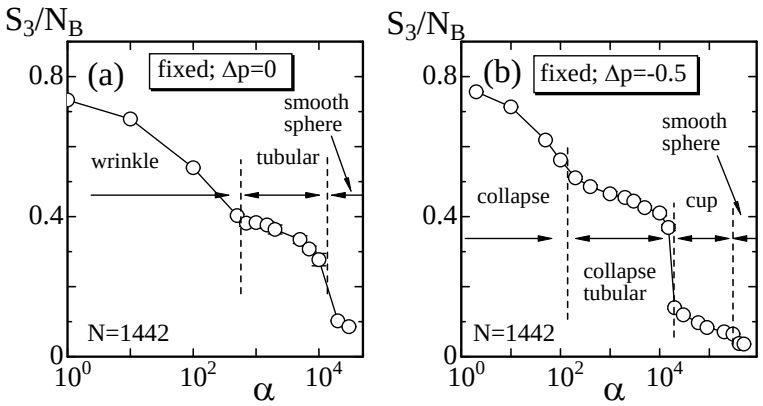

Fig. 9. The two-dimensional bending energy S_3/N_B vs. α under (a) $\Delta p=0$ and (b) $\Delta p=-0.5$.

The two-dimensional bending energy S_3/N_B is shown in Figs. 9(a) and 9(b),

where S_3 is defined by using a unit normal vector $\mathbf{n}_i$ of the triangle i such that

$$S_3 = \sum_{(ij)} (1 - \mathbf{n}_i \cdot \mathbf{n}_j). \tag{7}$$

We write the two-dimensional bending energy as S_3 to distinguish it with the deficit angle energy S_2 in Eq. (3).

We see that S_3/N_B discontinuously changes at the phase boundaries, where the physical quantities such as V, X^2 and L_E discontinuously change. To the contrary, the deficit angle energy S_2 defined in Eq. (3), which is not shown in the figures, appears to vary almost smoothly in the whole range of α. At the boundary between the smooth spherical phase and its neighboring phase, S_2/N is expected to change discontinuously like the other physical quantities. However, the discontinuity is very small and it is almost invisible just as in the case of the self-intersecting model in Ref. [29].

6. Summary and Conclusion

We have numerically studied a self-avoiding (SA) surface model on fixed-connectivity (FC) triangulated lattices of sphere topology. The self-avoidance of the model in this paper is not identical to those of the well-known SA models; the ball spring model and the impenetrable plaquette (IP) model. However, the SA model in this paper belongs to the IP models, because the intersection of disjoint triangles are prohibited by the SA interaction. The phase structure of the FC model under $\Delta p = 0$ is found to be almost identical to that of the phantom surface model in Ref. [29] except for the evidence that the collapsed phase disappears from the SA model. Thus, the influence of the SA interaction on the phase structure is very small contrary to the expectation that the SA interaction can suppresses the multitude of phase transitions in the phantom surface model.

To be more precise, the model in this paper is a Nambu-Goto surface model with a deficit angle energy. The SA interaction is defined such that all possible pairs of non-nearest neighbor triangles are prohibited from intersecting. Because the volume enclosed by the SA surface is well defined, the pressure term $-\Delta p\, V$ can be included in the Hamiltonian. The simulations are performed under $\Delta p = 0$, and $\Delta p = -0.5$ on the FC surfaces, where $\Delta p = -0.5$ implies that the pressure inside the surface is lower than the pressure outside the surface.

Our observations on the FC surfaces are as follows: the smooth spherical phase, the tubular phase, and the collapsed phase can be seen under those two conditions of Δp, and the cup like phase is seen under $\Delta p = -0.5$. Thus, the phase structure of the model under $\Delta p = 0$ is almost identical to that of the phantom surface model, although the collapsed phase is slightly different from each other; the collapsed surfaces are completely shrunk in the phantom surface model, while the SA surfaces are not completely shrunk at $\Delta p = 0$ at least. The Hausdorff dimension $H = 2.33(8)$, obtained at $\alpha = 0$ under $\Delta p = 0$, is independent of the curvature energy and is considered as the Hausdorff dimension of the Nambu-Goto SA surface. This result

is consistent with the known result of $H \simeq 2.3$ of the IP model in Ref. [38], where the model, the SA interaction, and the surface topology are different from those in this paper. In this sense, it is possible that the value $H \simeq 2.3$ depends only on the self-avoidance, although the surface size of the simulation in Ref. [38] is relatively smaller than those assumed in this paper. To the contrary, $H = 2.33(8)$ is larger than the result $H = 2.1(1)$ of Ref. [42], and therefore, it is also possible that H of the SA surface depends on the model. The SA surface models should be studied more extensively.

It is also interesting to study whether or not the multitude of phases in the fluid surface models with cytoskeletal structures in Ref. [27] is observed under a SA interaction. The SA interaction assumed in the model of this paper can also be assumed in those fluid surface models even when Δp is negative. This remains to be a future study.

References

1. D. Nelson, in *Statistical Mechanics of Membranes and Surfaces, Second Edition*, ed D. Nelson, T. Piran, and S. Weinberg, (World Scientific, 2004, Singapore), p 1.
2. G. Gompper and M. Schick, *Self-assembling amphiphilic systems*, In *Phase Transitions and Critical Phenomena 16*, ed Domb C and Lebowitz J L, (Academic Press, 1994, New-York) p 1.
3. K.J. Wiese, *Phase Transitions and Critical Phenomena 19*, ed C. Domb and J.L. Lebowitz, (Academic Press, 2000) p 253.
4. M. Bowick and A. Travesset, 2001 Phys. Rep. **344** 255.
5. U. Seifert, Fluid Vesicles, in *Lecture Notes: Physics Meets Biology. From Soft Matter to Cell Biology.*, 35th Spring School, Institute of Solid State Research, Forschungszentrum Jülich (2004).
6. G. Gompper and D.M. Kroll, in *Statistical Mechanics of Membranes and Surfaces, Second Edition*, ed D. Nelson, T. Piran, and S. Weinberg, (World Scientific, 2004, Singapore), p 359.
7. J.F. Wheater, 1994 J. Phys. A Math. Gen. **27** 3323.
8. W. Helfrich, Z. Naturforsch **28**c, 693 (1973).
9. A.M. Polyakov, Phys. Lett. B **103**, 207, 211 (1981).
10. A.M. Polyakov, Nucl. Phys. B **268**, 406 (1986).
11. H. Kleinert, Phys. Lett. B **174**, 335 (1986).
12. L. Peliti and S. Leibler, Phys. Rev. Lett. **54** (15), 1690 (1985).
13. M. Paczuski, M. Kardar, and D.R. Nelson, Phys. Rev. Lett. **60**, 2638 (1988).
14. F. David and E. Guitter, Europhys. Lett. **5** (8), 709 (1988).
15. J. -P. Kownacki and D. Mouhanna, Phys. Rev. E **79**, 040101 (R) (2009).
16. A. Billoire and F. David, Nucl. Phys. B **275** [FS17], 617 (1986).
17. D.V. Boulatov, V.A. Kazakov, I.K. Kostov, and A.A. Migdal, Nucl. Phys. B **275** [FS17], 641 (1986).
18. Y. Kantor and D.R. Nelson, Phys. Rev. A **36**, 4020 (1987).
19. A. Baumgärtner and J.S. Ho, Phys. Rev. A **41**, 5747 (1990).
20. S.M. Catterall, J.B. Kogut, and R.L.Renken, Nucl. Phys. Proc. Suppl. B **99**A, 1 (1991).
21. J. Ambjorn, A. Irback, J. Jurkiewicz, and B. Petersson, Nucl. Phys. B **393**, 157 (1993).

22. Y. Nishiyama, Phys. Rev. E **70**, 016101 (2004).
23. J. -P. Kownacki and H.T. Diep, Phys. Rev. E **66**, 066105 (2002).
24. H. Koibuchi, N. Kusano, A. Nidaira, K. Suzuki, and M. Yamada, Phys. Rev. E **69**, 066139 (2004).
25. H. Koibuchi and T. Kuwahata, Phys. Rev. E **72**, 026124 (2005).
26. I. Endo and H. Koibuchi, Nucl. Phys. B **732** [FS], 426 (2006).
27. H. Koibuchi, Phys. Rev. E **75**, 051115 (2007); Phys. Rev. E **76**, 061105 (2007).
28. H. Koibuchi, Euro. Phys. J. B **59**, 405 (2007).
29. H. Koibuchi, Z. Sasaki, and K. Shinohara, Phys. Rev. E **70**, 066144 (2004).
30. Koibuchi H, Euro. Phys. J. B **59**, 55 (2007).
31. Y. Kantor, M. Karadar and D.R. Nelson, Phys. Rev. Lett. **57**, 791 (1986).
32. Y. Kantor, M. Karadar and D.R. Nelson, Phys. Rev. A **35**, 3056 (1987).
33. M. Plischke and Boal, Phys. Rev. A **38**, 4943 (1988).
34. J. -S. Ho and A. Baumgärtner, Europhys. Lett. **12**, 295 (1990).
35. A. Baumgärtner, J. Phys. I (France) **1**, 1549 (1991).
36. A. Baumgärtner, Europhys. Lett. **17**, 381 (1992).
37. G. Grest, J. Phys. I (France) **1**, 1695 (1991).
38. D.M. Kroll and G. Gompper, J. Phys. France **3**, 1131 (1993).
39. G. Gompper and D.M. Kroll, Phys. Rev. E **51**, 514 (1995).
40. C. Münkel and D.M. Heermann, Phys. Rev. Lett. **75**, 1666 (1995).
41. M. Bowick, A. Cacciuto, G. Thorleifsson, and A. Travesset, Phys. Rev. Lett. **87**, 148103 (2001).
42. M. Bowick, A. Cacciuto, G. Thorleifsson, and A. Travesset, Euro. Phys. J. E **5**, 149 (2001).
43. N. Stoop, F. K. Wittel, M. B. Amar, M. M. Muller, and H. J. Herrmann, Phys. Rev. Lett. **105**, 068101 (2010).
44. J. Ambjorn, B. Durhuus, and J. Fröhlich, Nucl. Phys. B **257**, 433 (1985).
45. C.F. Baillie, and D.A. Johnston, 1993 Phys Rev. D **48** 5025; Phys. Rev. D **49**, 4139 (1994).
46. C.F. Baillie, D. Espriu, and D.A. Johnston, Phys. Lett. B **305**, 109 (1993).
47. C.F. Baillie, A. Irback, W. Janke, and D.A. Johnston, Phys. Lett. B **325**, 45 (1994).
48. H. Koibuchi, N. Kusano, A. Nidaira, Z. Sasaki, and T. Suzuki, Euro. Phys. J. B **42**, 561 (2004).
49. M. Igawa, H. Koibuchi, and M. Yamada, Phys. Lett. A **338**, 433 (2005).
50. I. Endo and H. Koibuchi, Phys. Lett. A **350**, 11 (2006).
51. F. David, Nucl. Phys. B **257** [FS14], 543 (1985).
52. H. Koibuchi, Euro. Phys. J. B **57**, 321 (2007).
53. D.H. Boal and U. Seifert, Phys. Rev. Lett. **69**, 3405 (1992).